Journal of Power Sources 196 (2011) 9481–9487

Contents lists available at ScienceDirect

Journal of Power Sources

journal homepage: www.elsevier.com/locate/jpowsour

A plate-frame flow-through microfluidic fuel cell stack

Sean Moore [a], David Sinton [b], David Erickson [a,*]

[a] Sibley School of Mechanical and Aeronautical Engineering, Cornell University, Ithaca, NY 14853-7501, USA
[b] Department of Mechanical Engineering, and Institute for Integrated Energy Systems (IESVic), University of Victoria, 3800 Finnerty Road, Victoria, BC V8W2Y2, Canada

ARTICLE INFO

Article history:
Received 26 May 2011
Received in revised form 6 July 2011
Accepted 7 July 2011
Available online 31 July 2011

Keywords:
Fuel cell
Plate-frame
Microfluidic
Membraneless
Carbonization
Electrode

ABSTRACT

We present a plate-frame microfluidic fuel cell architecture with porous flow-through electrodes. The architecture combines the advantages of recent microfluidic fuel cells with those of traditional plate-frame PEM fuel cells and enables vertical stacking with little dead volume. Peak current and power densities of 15.7 mA cm^{-2} and 5.8 mW cm^{-2} were observed. In addition to the new plate-frame architecture, microfabrication techniques have been used to create a new form of high performance electrode. Laser ablation of a polymer precursor followed by a pyrolysis process was used to create a thin, low-cost micro-porous electrode that provides for more rapid reactant transport. Here we show a 140% increase in power density compared to commercial carbon fiber paper.

1. Introduction

Rising power demands in portable electronics will require technical development of small and efficient power supplies in order to energize the next generation of portable devices. Microfluidic fuel cells are considered to be a technology with the potential to meet these demands [1–5]. In general liquid fuels have higher energy density than batteries while offering easy handling/storage, potentially reducing device size and increasing run time [6]. In addition, refueling offers virtually no downtime compared to recharging.

A microfluidic fuel cell incorporates all the fundamental components of a fuel cell into a microfluidic system, and typically operates without a proton exchange membrane (PEM) [7]. The diffusional interface between two miscible fluids that forms at low Reynolds numbers is used as a barrier; in some cases an additional electrolyte stream is used [8–10]. The colaminar flow streaming allows for a great degree of flexibility in fuel and oxidant choice. Membraneless devices have been demonstrated using formic acid [11–13], vanadium [14–16], ethanol [17], methanol [10,18], hydrogen [19,20]. Fuel cells generate power from surface reactions; here the high surface to volume ratios inherent in microfluidic devices is beneficial [4]. Removal of the need for a PEM eliminates difficulties with membrane/electrode fouling, water management and reactant cross-over. Removing these limitations serves to decrease maintenance and design cost. In addition, the material cost of the polymer membrane alone is significant.

Kjeang et al. [7] identified several key challenges which need to be addressed for microfluidic FCs to be commercialize, one of them being scaling of these systems. Power output of a single microfluidic fuel cell is insufficient for most applications and most applications require multiple independent cells. Both space and weight are at a premium in portable electronic devices therefore power sources must be both volumetrically and gravimetrically efficient. Robust, space-efficient designs which are easily scaled to meet a variety of power requirements are needed. To date, most laminar flow fuel cells have been fabricated using soft lithography techniques, with the cell placed on a two-dimensional substrate.

While excellent for prototype demonstrations, the volumetric costs of additional substrates and fluid handling networks limits the expansion of this these cells. Volumetric efficiency of these microfluidic cells is limited by sealing and structural elements. Some work has been done in expanding cell architecture into working 3-D devices with low dead space. Cohen et al. [13] for example demonstrated a two cell stack of their planar architecture. In that work, fuel (formic acid) and oxidant (dissolved O_2) streams were layered vertically. This device used planar platinum electrodes patterned on the top and bottom substrates. The performance of parallel flow based designs with planar electrodes is typically limited by mass transport across the diffusive boundary layer that

Abbreviations: PEM, polymer electrolyte membrane; CFP, carbon fiber paper.

* Corresponding author at: Sibley School of Mechanical and Aeronautical Engineering, 240 Upson Hall, Cornell University, Ithaca, NY 14853-7501, USA.
Tel.: +1 607 255 4861; fax: +1 607 255 1222.
E-mail address: de54@cornell.edu (D. Erickson).

0378-7753/$ – see front matter © 2011 Elsevier B.V. All rights reserved.
doi:10.1016/j.jpowsour.2011.07.024

forms over the electrodes, and broadening of the fuel/oxidant interface. The powers of these fuel cells were restricted to about 1 mW by mass transport and the solubility of dissolved oxygen. Kjeang et al. [14] showed a novel 3-D architecture using graphite rods arrange in a hexagonal array and vanadium redox chemistry. Their device is readily scaled in both the horizontal and the vertical direction; although the vertical is preferred. The cylindrical electrodes used in that case were essentially planar electrodes rolled along one axis; mass transport across the growing diffusive boundary layer on the surface limited cell performance. Later Kjeang et al. [15] developed a microfluidic fuel cell with flow-through porous electrodes that improved performance due to improved reactant transport. The design, however, was planar in nature and was not well suited to integration in a stack. Recently Salloum and Posner [21] demonstrated a fuel cell with a planar multipass configuration analogous to a conventional PEM fuel cell stack. Their work also used carbon fiber paper electrodes in a flow-through configuration where cells were arranged in plane and showed improved fuel utilization compared to a single pass cell. Flow through electrodes maximize reaction surface and reduce mass transport losses. The requirement of an addition of an electrolyte stream complicates the device and the use of a 2-D planar substrate increases the overhead space required for stacking these cells [7].

Individual cell performance is limited by a combination of losses due to the electrochemical kinetics, ohmic resistance, and species transport [7]. Species transport to and from the active sites occurs primarily by convection and diffusion [7]. This can be enhanced by increasing reactant concentration, flow velocity, or reducing the average cross-stream distance. Electrode configuration and structure are inherently connected to cell performance via mass transport losses. Commercially available carbon fiber paper (CFP) is cheap and has shown excellent performance in both flow-over, and flow-through configurations [8,11,12,15,21,22]. The use of porous electrodes allows for higher power densities while maintaining increased single pass fuel utilization.

Here we present a novel membraneless plate-frame architecture constructed using rapid prototyping, self-supported carbon electrodes, and using vanadium redox chemistry. This approach offers a robust, simple, readily expanded architecture which capitalizes on the advantages presented by flow through electrodes while requiring little overhead volume. Bipolar plates commonly used in PEM fuel cells have the advantage of acting as both a structural and electrical component. Here our electrodes are self-supporting and arranged in a similar fashion with the exception that reactants flow through the electrode structure, normal to the plane of the plates. A schematic depicting the fluidic and electrode configuration of our plate-frame architecture is shown in Fig. 1. Electrodes are aligned horizontal to one another and separated by electrolyte. Fuel and oxidant flow is distributed vertically through the electrodes. The fluidics are defined by the polymer manifolds which are well-suited to low cost mass production techniques such as injection molding. The manifolds are symmetric except for the inlet channel and are simply rotated upon assembly to incorporate the appropriate fluidic streams. Using identical manifolds, the overall part count, and subsequently manufacturing cost are minimized. We characterize cell performance as a function of reactant flow rate and electrode thickness. A two cell stack is also demonstrated. The plate-frame architecture described here is also used to test a new form of microfabricated electrode. These electrodes were patterned in polyimide using laser ablation and then carbonized by pyrolysis. Pore size in these electrodes is significantly smaller than the carbon fiber paper used to characterize the architecture. Decreasing pore size within the electrode reduces the cross stream diffusion distance and benefits from increased reaction surface area. The high cross sectional area and low electrode thickness of the plate-frame architecture increases

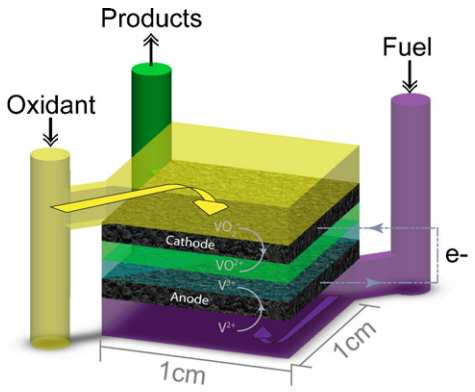

Fig. 1. Internal fluidic geometry of the plate-frame microfluidic fuel cell architecture. Oxidant, VO_2^+ is shown in yellow and Fuel, V^{2+} is shown in purple. The product species, V^{3+} and VO^{2+} are showing in blue and green respectively. The porous electrodes (gray) are separated by product streams. Current path is completed by wire leads external to the cell. The cell is shown here is being discharging. (For interpretation of the references to color in text, the reader is referred to the web version of the article.)

electrode area normal to the flow and reduces electrode thickness. This geometry limits pumping losses through the porous media, allowing for thin, microporous electrodes, and reduces cell volume.

2. Fabrication and experimental methods

Fabrication and testing of our membraneless plate-frame architecture with flow through electrodes is described here. A sketch of the internal geometry of our device is shown in Fig. 1. Here the co-laminar streams are layered vertically and the liquid–liquid interface is horizontal. The design is made of stacking polymer manifolds, which simultaneously serve to house the electrodes and define the fluidics through the fuel cell. The fluidics consists of two fluidic supply channels and an exit port 1.5 mm in diameter. These feed into additional cells by flowing downward through the plate, or into a fluidic reservoir between electrodes. The porous electrode, shown in gray/black, serves as the catalyst and current collector. The exposed area of the electrode is 1 cm^2 and all the results presented here have been normalized with this area. The electrodes are spaced 1.5 mm apart; a 1 mm slot in the plate provides contact between the streams for proton conduction. To simplify the fabrication and experimentation the cells were sealed by external clamps; however a final manufactured product could be permanently sealed to reduce overhead space. We used two different kinds of electrodes with this architecture; commercially available carbon fiber paper (CFP) and micro fabricated electrodes.

2.1. Chemistry

In this work we have chosen to use vanadium redox species. The all vanadium redox cell uses oxidized vanadium ions for fuel (V^{2+}) and oxidant (VO^{2+}). This chemistry benefits from balanced and rapid reaction kinetics on plain carbon substrates; the fuel and oxidant are easy to prepare and offer high electrochemical potentials. This makes vanadium redox chemistry appealing for testing new architectures. Vanadium redox chemistry is limited by stability of oxidized vanadium in solution. Typically 2 M solutions are used although stability at higher concentrations has been shown [23]. Compared to liquid hydrocarbon fuels, vanadium redox solutions are less energy dense.

Vanadium based fuel (V^{2+}) and oxidant (VO_2^+) solutions were prepared using the following method. A 2 M sulfuric acid supporting electrolyte, prepared from DI water (Millipore) and concentrated sulfuric acid (Mallinckrodt Chemicals). Vanadium (IV)

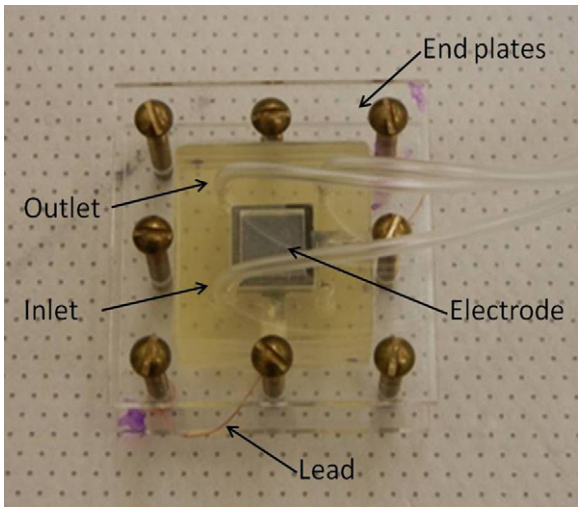

Fig. 2. The assembled cell uses acrylic end plates and bolts to provide sealing. Fluidic manifolds and electrode (black) are layered and centered in the end plates.

oxide sulfate hydrate ($VOSO_4{\cdot}xH_2O$, Alfa Aesar) was dissolved into the supporting electrolyte at 60 °C with constant stirring until a light blue solution of VO^{2+} at a concentration of 2 M was obtained.

An electrochemical cell, built in house, was used to prepare the fuel (V^{2+}) and oxidant ($VO_2{}^+$). The cell was machined from Teflon and utilizes a Nafion (N-212, DuPont) proton exchange membrane and carbon fiber paper electrodes (Spectracarb 2050-A). Nitrogen gas was bubbled into and out of the cell due to the instability of V^{2+} with oxygen. Sealing was accomplished using a rubber (butane-n) gasket. To initially charge the fuel and oxidant solutions, 60 ml of VO^{2+} is added to the positive half-cell while 30 ml is added to the negative half-cell and 1.9 V is applied across the cell. The solution were considered "charged" after reaching −0.52 and +0.94 V vs. Ag/AgCl in the anodic and cathodic solutions respectively, giving redox concentration ratios of 93% V^{2+} and 99% $VO_2{}^+$. When the fuel and oxidant solutions were regenerated from previous experiments, fresh VO^{2+} solution may be added to one of the half-cells to obtain proper final concentrations. To limit degradation due to oxygen contamination, the fuel and oxidant solutions were used shortly after charging and not stored.

2.2. Cell fabrication

A schematic of the fuel cell and picture of the assembled cell is shown in Figs. 1 and 2 respectively. The cell consists of several fluidic manifolds, acrylic end plates, and carbon electrodes all of which were fabricated in-house. The fuel cell manifolds were printed in FullCure 720 on a Connex 500 (Objet) 3D printer. The acrylic end plates, used to sandwich the cell, were cut from 3 mm acrylic sheets with a CO_2 laser cutter/engraver (Versalaser). Tygon tubes were inserted into the top end plate to provide flow into and out of the cell. Paraffin film gaskets and wax were used to seal the manifolds and electrode connections. After assembly the cell was heated at 80 °C for 10 min. Bolts connecting the acrylic end plates were then tightened, deforming the softened paraffin to seal the cell. Connection to each electrode was provided using silver conductive epoxy.

2.3. Electrode fabrication

Carbon fiber paper electrodes were cut from Spectracarb or Toray carbon fiber sheets with thicknesses of 0.37 mm and 0.25 mm respectively. Electrodes of 1.0 mm and 3.0 mm were fabricated by stacking 4 sheets of Spectracarb and 8 sheets of Toray fiber paper. These were joined at the connection tab by silver conductive epoxy.

The microfabricated electrodes were made from a 0.1 mm thick Kapton (DuPont) polyimide precursor. First, the precursors were cut and patterned with a CO_2 laser cutter/engraver (Versalaser). Single laser pulses were used to create pores in the film while the outside was cut by raster scanning the laser. The precursors were carbonized by pyrolysis in a nitrogen tube furnace. Polyimide was chosen because of its aromatic structure which readily forms glassy carbon during pyrolysis in an inert environment [21,22]. The films were first heated to and held at 400 °C for 1 h. Afterwards the temperature was increased at a rate of 2 °C min^{-1} to 600/800 °C and held for 1 h to complete the pyrolysis process. Scanning electron micrographs of the microfabricated electrodes are shown in Fig. 7. The laser is pulsed once per pore and the pore size is determined by intensity, laser spot size, and shrinkage during pyrolysis. Due to an approximately 30% shrinkage in the film area during pyrolysis a final pore size of 29 μm was achieved. Here the pore size is limited by the 31 μm spot size of the laser. The pore size showed little variability across the 1 cm × 1 cm electrode surface when imaged under SEM. Spacing is set by the DPI of the laser printer and shrinkage of the film due to pyrolysis. Here pores are arranged in a square grid with ~200 μm spacing. Other types and closer spacing's are possible, only limited by the structural integrity of the film. In future, increasing the pore count would act to increase electrode surface area while decreasing pumping losses.

2.4. Fuel cell diagnostics

Flow of fuel and oxidant solution were provided by a syringe pump at rates from 3 ml h^{-1} to 0.05 ml h^{-1} and delivered to the cell via Tygon tubing. Polarization data was gathered using a Keithley 2400 source meter by chronoamperometry. Voltages were swept from open to close circuit at a rate of 1.4 mV s^{-1}, which was determined to be below the response time of the cell. The combined ohmic resistances of the cells were found by current interrupt.

3. Results and discussion

In this section we present polarization results characterizing the plate-frame architecture at different flow rates, electrode thicknesses and electrode materials. Using CFP electrodes, result of single cell operation are compared to two cells stacked fluidically and electrically in parallel. Performance of micro fabricated electrodes is compared to the previous results.

3.1. Plate-frame architecture

Steady state polarization curves were measured at room temperature under potentiostatic control. The average open circuit potential (OCP) was found to be 1.34 ± 0.05 V. This is 0.12 V less than the maximum OCV given the fuel and oxidant solutions which is most likely due to a small amount of reactant crossover across the parallel streams and manifold. This result is on par with the array architecture described by Kjeang et al. [14], however it is below single cell results [15,16,22]. CFP electrodes were used to characterize the device and the effect of flow rate and electrode thickness on system performance was studied. The polarization curves shown in Fig. 3 were recorded at flow rates of 0.05, 0.1, and 3 ml h^{-1}. The Reynolds number here is given by $Re = U_o b/\upsilon$, where U_o is the mean fluid velocity, b is half the distance between electrodes, and b is the kinematic viscosity, was found to be approximately 0.1 at the stream interface for the maximum flow rate used. This insures limited fuel cross over across the product streams. Current and power densities up to 15.7 mA cm^{-2} and 5.8 mW cm^{-2} respectively, were observed. Several trends are shown here in Fig. 3. As expected, both

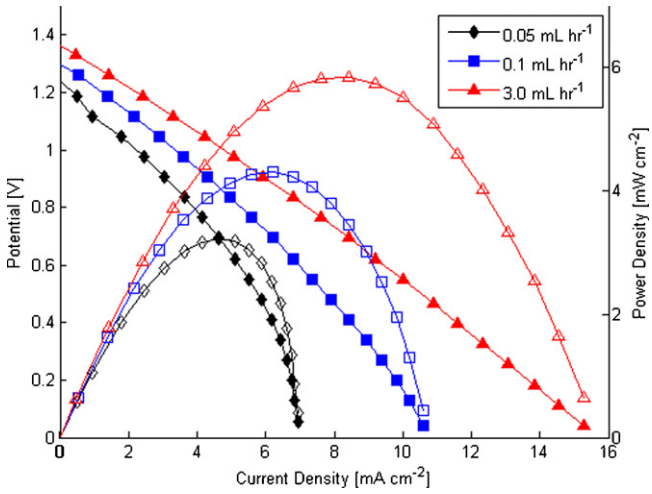

Fig. 3. Polarization and power curves for three flow rates through the cell with CFP electrodes: 0.05, 0.1, and 3.0 ml h^{-1}. The electrode thickness here is 3 mm. Here closed symbols correspond to the primary vertical axis, voltage. Open symbols correspond to the secondary vertical axis, power density.

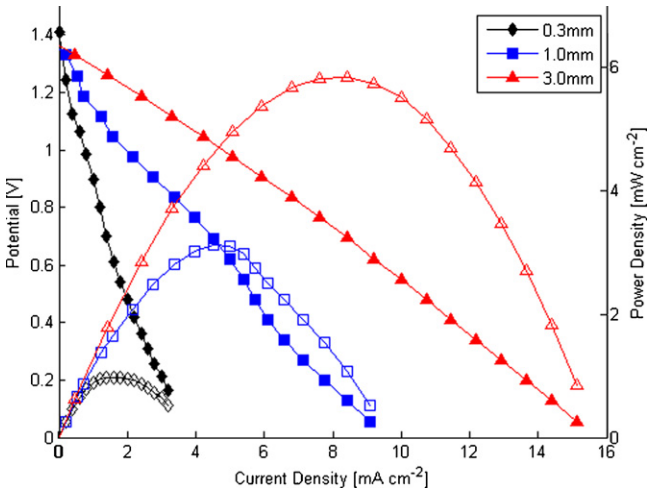

Fig. 4. Polarization and power curves for three thicknesses of CFP electrode: 0.3 mm, 1.0 mm and 3 mm. Fuel and oxidant flow rate was set to 3 ml h^{-1}. Here closed symbols correspond to the primary vertical axis, voltage. Open symbols correspond to the secondary vertical axis, power density.

power and current density increase with increasing flow rate due to increased convective transport. At the lower flow rate, there is a steep drop in voltage at higher current densities due to mass transport limitations. Fuel cross over is also a concern at lower flows as the 0.1 V drop in OCP indicates. Due to the relatively large electrode gap of 1.5 mm, omhic losses are a concern in this design. Here we see decreased returns for increasing flow rate as well as nearly linear polarization curves which implies a high internal resistance in the cell. The combined ohmic resistance for the cell is the total series resistance of the electrolyte, electrodes, wire leads, and contacts. The cell resistance was estimated using current interrupt though some correction is required when using this technique with porous electrodes [24,25].

$$\Delta V_{\Omega} = \frac{L}{k_{\text{electrolyte}} + k_{\text{electrode}}} i \tag{1}$$

Here ΔV_{Ω} is the voltage correction due to potential gradients within the electrodes at the pre-interrupt condition, L is the electrode thickness, $k_{\text{electrolyte}}$ and $k_{\text{electrode}}$ are the effective conductivities of the electrode and electrolyte respectively. The ohmic resistance measured by current interrupt was $98.0 \pm 2.3\ \Omega$ at a flow of 3 ml h^{-1}, this value is larger than previous work [14,15,21]. The omhic resistance estimated using the slope of the polarization curve is 132.3 Ω; this assumes all losses are ohmic. At 3 ml h^{-1} the majority, 76%, of the loss in the cell is from ohmic resistance. Losses due to the total cell resistance severely hinder the performance of this design and need to be addressed by lowering the electrode gap, switching to a higher conductivity electrolyte, or redesigning the system. One simple solution would be to increase the cross sectional area of the electrolyte conduction path. Due to the high ohmic resistance the power out-put of our device is considerably lower than previously reported results [14,15,21,22]. The plate frame architecture provides a simple, low volume way to stack cells fluidically in parallel with the benefits of flow through electrodes. The internal ohmic resistance must be reduced in order to achieve a viable device.

We investigate the effect of increasing electrode thickness as shown in Fig. 4. Increasing electrode thickness was found to improve performance, by increasing the active surface area. Electrode thickness was varied by stacking multiple layers of carbon fiber paper together. Fig. 4 shows polarization and power curves for three thicknesses (0.3, 1.0, 3.0 mm) at a flow rate of 3 ml h^{-1}. The increase in current and power density is due to increased fuel utilization, which is defined as follows.

$$\eta = \frac{iA}{nFCQ} \tag{2}$$

Here η is the fuel utilization, Q is the volumetric flow rate, n is the number of electrons per reaction, C is the reactant concentration, and A, i, F are defined as before. Here the fuel utilization is load dependent. Although fuel utilization is higher under low load, little power is produced. Due to its variability it is important to exam fuel utilization under a realistic operating condition. The peak power for all cases, as shown in Figs. 3 and 4, occurs close to 0.8 V; fuel utilization will be discussed at this operating point. As seen in Fig. 5, fuel utilization depends significantly on electrode thickness, and as expected increases with decreasing flow rates. At 0.8 V up to 66% of the primary reactants are used. At low voltages, low flow rates, and with 3 mm thick electrodes we observe over 100% fuel utilization, similar to the results reported by Kjeang et al. [15]. This is due to the secondary vanadium redox couple. The dependence on electrode thickness and flow rates are both related to the reactant transport within the electrode. At lower flow rates reactant species have more time to diffuse to the electrode surface and react. At higher electrode thicknesses, the same is true. In this regard there is a clear trade off in power output and pumping loss in the cell; and it is likely that significant gains would be possible by optimizing this system through modeling and experimentation (Fig. 5).

Similar to plate frame PEM cells, the architecture used here allows individual cells to be easily stacked together; however, the traditional bipolar plate configuration cannot be used here. This is due to the flow-through electrode configuration; electrodes with the same potential sandwich the fuel or oxidant reservoirs. Flow of reactants is either upward or downward through the electrode depending upon location. Fig. 1 only shows a part of the unit cell whereas a full unit cell consists of 4 electrodes, 2 reactant reservoirs, and 2 colaminar streams. The electrodes must be connected externally and can be configured for series or parallel operation. Multi-cell performance testing of two cells arranged in parallel is shown in Fig. 6. Here we see individual cell performance is maintained, and both cells operate well independently of each other. The cells here are wired together in parallel, as expected the total current is the sum of the two cells. Since connections to each electrode are made externally, the device can easily be run in series, or

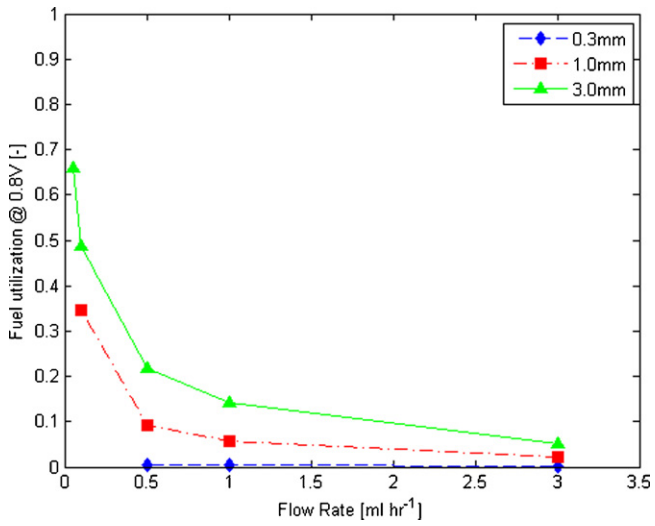

Fig. 5. Dependence of fuel utilization (η) on flow rate and CFP electrode thickness.

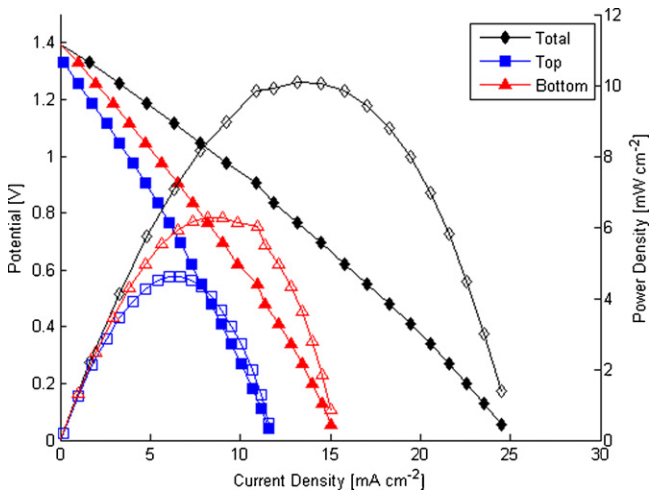

Fig. 6. Polarization and power curves for a two cells wired in parallel. Closed symbols correspond to the primary vertical axis, voltage. Open symbols correspond to the secondary vertical axis, power density. The flow rate was set to 6.0 ml h^{-1} into the two cells.

dynamically in response to a load. Series operation combines the cell voltage. At 0.8 V a 30% difference in current density is observed here, most likely due to small differences in flow rates between cells. Equivalent to electrical resistors in parallel, a change in fluidic resistance will alter the flow in one cell relative to another. Small differences in the electrodes, which are cut individually are likely responsible for this effect and improvements in manufacturing of the electrodes would mitigate this issue. It is noteworthy that the challenges associated with two phase flow in PEM fuel cells are not an issue in the all-liquid microfluidic fuel cell developed here.

3.2. Micro-fabricated electrodes

Electrode structure and pore size plays a large role in cell performance. Small pores decrease the diffusion distance required for reactants to reach the electrode surface, however smaller pore sizes tend to increase pumping losses. The tradeoffs associated with the latter are however small in comparison to the power gains. Here we have applied micro-fabrication techniques to a polymer precursor, which is carbonized via pyrolysis to form a carbon electrode with reduced pore size. Surface composition and conductance

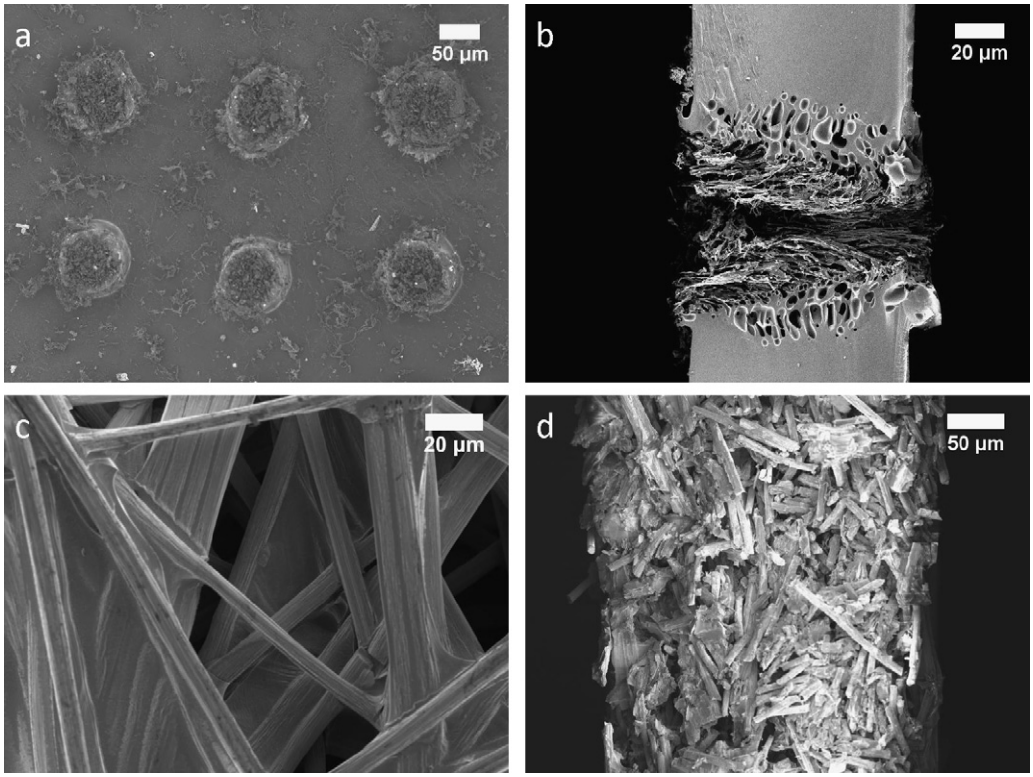

Fig. 7. Scanning electron micrographs of μfab electrodes and Spectracarb 2050-A carbon fiber paper. Top and cross-sectional views of the microfabricated electrodes are shown in a and b respectively, while top and cross-sectional views of the CFP are shown in c and d respectively.

Table 1
Summary of mass composition from XPS peaks after pyrolysis.

	O1s	C1s	N1s	Si 2p
Reported values	19.46	76.97	4.54	–
Control	17.95	75.58	5.08	1.12
600 °C	14.7	81.25	3.5	0.56
800 °C	8.68	89.22	1.88	0.24

are critical factors in electrode performance. For the microfabricated electrodes both are dependent on the pyrolysis conditions; including the temperature, dwell time, heating rate, and gas environment. During pyrolysis, volatile compounds such as H_2, O_2, CO, CO_2 and N_2 are formed and baked out, leaving a glossy carbon film. Vanadium redox chemistry is known to occur readily on carbon surfaces [26]. Pyrolysis of polyimide yields loosely organized graphite structures at low temperatures [27]. This gives conductive films without requiring additional furnace processing at higher temperatures, around 2000 °C. XPS results are shown in Table 1. A 51.6 and 63.0% drop in O1s and N1s peaks for samples processed at 800 °C is observed. In all cases a small amount of silicon contamination is observed. Silicon is commonly used in the fabrication facility and the material may have been picked up while handling the films. Both sets of samples appear to be glossy carbon, although significant differences in the chemical composition are measured in the XPS. This is reflected in the sheet resistance measurements. The electrode also serves as the current collector; high resistivity will negatively impact cell performance. At 600 °C the temperature was too low to properly carbonize the polyimide, as can be seen in Table 1. Due to the high resistance of these samples, accurate sheet resistance values could not be recorded. Four point probe sheet resistance measurements for the 800 °C samples show reasonable values, 4.71 Ω sq, compared to the CFP. The sheet resistance for both commercial carbon fiber sheets was 0.453 ± 0.05 Ω sq. It is expected that additional furnace processing at higher temperatures would further decrease the resistance. However, as the resistance is of the electrodes was found to be small compared to the electrolyte (as will be shown later), these processing conditions were considered suitable for our purposes and, all subsequent microfabricated electrodes were pyrolised at 800 °C (Fig. 7).

We used the same plate frame device to test the microfabricated electrodes. A polarization and power curve taken at 3 ml h^{-1} is shown in Fig. 8. Again, the *I*/*V* curve was nearly linear indicating strong ohmic loss, primarily due to the large electrode gap. Compared to CFP electrodes with over double the thickness (0.25 mm), a 140% increase in power density is observed as well as a 6 fold increase in fuel utilization. Here the reduced size scales within the electrode enhanced convective/diffusive species transport. The fabrication technique shown here is simple and robust; however, other techniques and more complex shapes can be applied in carbon [28–30]. Recent modeling work has shown the importance of electrode porosity to cell performance [31]. Using the method developed here, electrodes could be tailor made to suit the needs of a variety of architectures. The material properties of these two materials, such as porosity, pore size distribution (PSD), effective diffusion coefficient, and permeability were not examined. These properties should be measured in future works, in order to better characterize electrode materials and pin-point what modifications can be made to best improve performance. These results highlight the potential of applying microfabrication techniques to the electrode to improve reactant transport and improve performance.

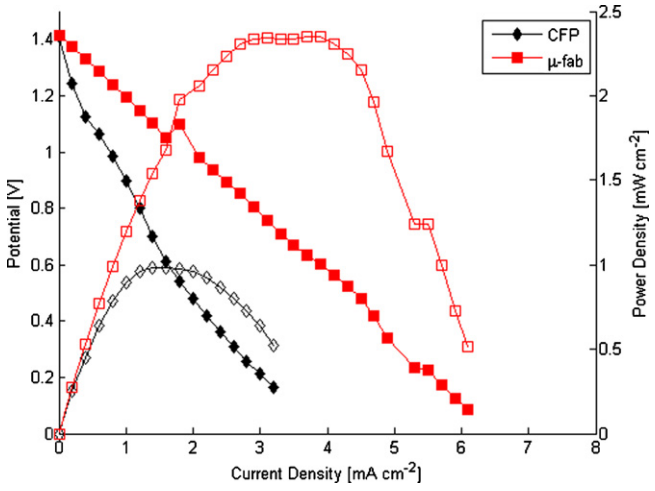

Fig. 8. Comparison of polarization and power curves for a cell equipped with single layer CFP or μfab electrodes. Fuel and oxidant flow rate was set to 3 ml h^{-1}.

4. Conclusions

In order to achieve useful power output from fuel cell systems, multiple fuel cells in series are required. In this work we developed plate-frame membraneless fuel cell with flow through electrodes. The architecture combines the advantages of recent microfluidic fuel cells with those of traditional plate-frame PEM fuel cells and enables stacking with little dead volume. Prototype fuel cells exhibited peak current and power densities of 15.7 mA cm^{-2} and 5.8 mW cm^{-2}. The performance of these prototype fuel cells was found to be limited predominantly by high ohmic resistance through the electrolyte. Operation of the cells in a stack was demonstrated, and the output of a two cell stacked in parallel was double that of a single cell.

To improve on this design, the plate-frame architecture developed here was used as a test platform for new microstructured electrodes. Microfabrication techniques were used to create electrodes with reduced internal dimensions. Laser ablation of a polymer precursor followed by a pyrolysis process was used to create a thin, low-cost micro-porous electrode that provides rapid reactant transport. These electrodes showed improved performance over the more commonly used CFP material at similar electrode thicknesses. This result highlights the potential of reducing size scales within the electrode to enhance species transport to the active surface and improve performance.

Acknowledgements

The authors would like to thank Vlad-Victor Oncescu for discussions, Richard Anger for fabrication support, and Mekala Krishnan for writing assistance. This work was done in part at the Cornell NanoScale Facility, a member of the National Nanotechonology Infrastructure Network, supported by the US National Science Foundation. Funding for the author was provided by the Graduate Research Fellowship Program, a part of the US National Science Foundation.

References

[1] D. Dunn-Rankin, E.M. Leal, D.C. Walther, Progress in Energy and Combustion Science 31 (5–6) (2005) 422–465.
[2] C.K. Dyer, Journal of Power Sources 106 (1–2) (2002) 31–34.
[3] J.D. Morse, International Journal of Energy Research 31 (6–7) (2007) 576–602.
[4] Lab on a Chip 7 (10) (2007) 1234–1237.
[5] J.W. Lee, E. Kjeang, Biomicrofluidics 4 (4) (2010) 041301–041312.
[6] G.H. Miley, et al., Journal of Power Sources 165 (2) (2007) 509–516.
[7] E. Kjeang, N. Djilali, D. Sinton, Journal of Power Sources 186 (2) (2009) 353–369.
[8] K.S. Salloum, J.D. Posner, Journal of Power Sources 195 (19) (2010) 6941–6944.
[9] J. Phirani, S. Basu, Journal of Power Sources 175 (1) (2008) 261–265.
[10] R.S. Jayashree, et al., Journal of the American Chemical Society 127 (48) (2005) 16758–16759.
[11] K.S. Salloum, et al., Journal of Power Sources 180 (1) (2008) 243–252.

[12] E. Kjeang, et al., Electrochimica Acta 54 (2) (2008) 698–705.
[13] J.L. Cohen, et al., Journal of Power Sources 139 (1–2) (2005) 96–105.
[14] E. Kjeang, et al., Journal of Power Sources 168 (2) (2007) 379–390.
[15] E. Kjeang, et al., Journal of the American Chemical Society 130 (12) (2008) 4000–4006.
[16] R. Ferrigno, et al., Journal of the American Chemical Society 124 (44) (2002) 12930–12931.
[17] C.M. Moore, S.D. Minteer, R.S. Martin, Lab on a Chip 5 (2) (2005) 218–225.
[18] E.R. Choban, et al., Journal of Power Sources 128 (1) (2004) 54–60.
[19] S.M. Mitrovski, R.G. Nuzzo, Lab on a Chip 6 (3) (2006) 353–361.
[20] S. Wagner, et al., Journal of Power Sources 190 (1) (2009) 76–82.
[21] K.S. Salloum, J.D. Posner, Journal of Power Sources 196 (3) (2011) 1229–1234.
[22] E. Kjeang, et al., Electrochimica Acta 52 (15) (2007) 4942–4946.
[23] F. Rahman, M. Skyllas-Kazacos, Journal of Power Sources 189 (2) (2009) 1212–1219.
[24] K.R. Cooper, M. Smith, Journal of Power Sources 160 (2) (2006) 1088–1095.
[25] C. Lagergren, G. Lindbergh, D. Simonsson, Journal of the Electrochemical Society 142 (3) (1995) 787–797.
[26] H. Kaneko, et al., Electrochimica Acta 36 (7) (1991) 1191–1196.
[27] J. Su, A.C. Lua, Journal of Membrane Science 305 (1–2) (2007) 263–270.
[28] L. Vogelaar, et al., Advanced Materials 15 (16) (2003) 1385–1389.
[29] L. Vogelaar, et al., Small 1 (6) (2005) 645–655.
[30] O.J.A. Schueller, S.T. Brittain, G.M. Whitesides, Sensors and Actuators A: Physical 72 (2) (1999) 125–139.
[31] A.E. Khabbazi, M. Hoorfar, ASME Conference Proceedings 2010 (44045) (2010) 659–665.